vRNA-vRNA interactions in influenza A virus HA vRNA packaging

Sho Miyamoto[1,2], Yukiko Muramoto[1], Keiko Shindo[1,3], Yoko Fujita[1,4], Takeshi Morikawa[1,4], Ryoma Tamura[1,4], Jamie L Gilmore[1], Masahiro Nakano[1,4], Takeshi Noda[1,4*]

[1] Laboratory of Ultrastructural Virology, Institute for Frontier Life and Medical Sciences, Kyoto University, Kyoto, Japan

[2] Department of Molecular Virology, Graduate School of Medicine, Kyoto University, Kyoto, Japan

[3] Keihanshin Consortium for Fostering the Next Generation of Global Leaders in Research, Kyoto, Japan

[4] Laboratory of Ultrastructural Virology, Graduate School of Biostudies, Kyoto University, Kyoto, Japan

* Corresponding author

18 E-mail: t-noda@infront.kyoto-u.ac.jp (TN)

19

Abstract

The genome of the influenza A virus is composed of eight single-stranded negative-sense RNA segments (vRNAs). The eight different vRNAs are selectively packaged into progeny virions. This process likely involves specific interactions among vRNAs via segment-specific packaging signals located in the 3' and 5' terminal coding regions of vRNAs. To identify vRNA(s) that interact with hemagglutinin (HA) vRNA during genome packaging, we generated a mutant virus, HA 5m2, which possessed five silent mutations in the 5’ packaging signal region of HA vRNA. The HA 5m2 virus had a specific defect in HA vRNA incorporation, which reduced the viral replication efficiency. After serial passaging in cells, the virus acquired additional mutations in the 5’ terminal packaging signal regions of both HA and PB2 vRNAs. These mutations contributed to recovery of viral growth and packaging efficiency of HA vRNA. A direct RNA-RNA interaction between the 5' ends of HA and PB2 vRNAs was confirmed *in vitro*. Our results indicate that direct interactions of HA vRNA with PB2 vRNA via their packaging signal regions are important for selective genome packaging and

enhance our knowledge on the emergence of pandemic influenza viruses through genetic reassortment.

Introduction

The genome of the influenza A virus consists of eight segmented, single-stranded, negative-sense viral RNAs (vRNAs). Each vRNA contains a central coding region in an antisense orientation. This region is flanked by segment-specific noncoding regions and common terminal promoter sequences. Each vRNA forms a helical, rod-shaped ribonucleoprotein complex (vRNP) that associates with multiple nucleoproteins (NPs) and with a heterotrimeric RNA-dependent RNA polymerase complex composed of PB2, PB1, and PA proteins. The vRNP is responsible for transcription and replication of constituent vRNA. Recent studies examining NP-vRNA interactions in the context of vRNPs have shown that the NPs bind to vRNA nucleotides non-uniformly without sequence specificity[1, 2], suggesting that some parts of the vRNAs are free of NPs, and can potentially form secondary or tertiary structures that protrude from the surface of rod-shaped vRNPs.

There is evidence to suggest that progeny virions selectively package each copy of the eight vRNAs. In virions, the eight different vRNPs

are arranged in a specific '1+7' pattern, where one vRNP is surrounded by the other seven vRNPs[3, 4]. The mechanism by which each copy of the eight vRNAs is selected from a large pool of vRNAs and non-viral RNAs in virus-infected cells, and how these vRNAs are organized into the specific '1+7' arrangement, remains unclear. The segment-specific packaging signal sequences, located in the noncoding and terminal coding regions of both the 3' and 5' ends of each vRNA, likely ensure the integrity of genome packaging[5-10]. The terminal coding regions within these packaging signal sequences are thought to be involved in co-packaging of multiple vRNAs, and are referred to as bundling signals [11]. Mutations or deletions in bundling signal sequences reduce the packaging efficiency of several vRNAs. The impact of such mutations or deletions on packaging efficiency is hierarchical among the eight vRNAs[8, 12-19], suggesting that there are specific interactions among the vRNPs. The vRNPs form sub-bundles *en route* to the plasma membrane [20, 21], and vRNPs in virions are directly or indirectly interconnected with each other[22, 23]; these findings offer additional evidence for the existence of vRNA-vRNA interactions.

To further examine the likely involvement of vRNA-vRNA interactions in genome packaging, it is necessary to identify which vRNA segments interact with one another, and which regions of each vRNA segment participate in these interactions. The potential *in-vitro* interactions of various naked vRNA segments have previously been described in human H3N2 and avian H5N2 viruses [22, 24]. However, the various combinations of vRNA-vRNA interactions differ between the two viruses. It also remains unclear whether such *in-vitro* vRNA-vRNA interactions in the absence of NPs reflect interactions that may occur among vRNPs *in vivo*. Only some nucleotides that are important for vRNA-vRNA interactions have been identified in the context of virus replication in cells and co-packaging into virions[22, 25]. These studies suggest that the 5' ends of M vRNA and the central coding region of PB1 vRNA are involved in interactions and co-packaging with NA vRNA, respectively. In addition, interactions between PB1 and NS vRNAs may also be necessary for efficient viral replication and genome packaging. However, the region in NS vRNA identified to interact with PB1 vRNA is not located in the region of the previously reported

genome packaging signal [26]. Thus, the role of vRNA-vRNA interactions in genome packaging remains unclear.

In this study, we used serial passaging to identify which vRNA(s) interact with the hemagglutinin (HA) vRNA packaging signal in selective genome packaging. We first generated a mutant influenza virus (A/WSN/33) that possesses five silent mutations in the packaging signal of HA vRNA, which causes a specific defect in the incorporation of HA vRNA. Then, we serially passaged the mutant virus in cultured cells to restore efficient incorporation of HA vRNA, and identified mutations that had been newly introduced into the vRNAs. In addition, we examined the interactions of HA vRNA with potential partner vRNAs *in vitro*, and assessed the importance of these vRNA-vRNA interactions in the packaging signal regions specific for HA vRNA incorporation and viral replication.

Results

Generation of mutant viruses possessing silent mutations in the packaging signal of HA vRNA.

We first disrupted the packaging signal sequence of HA vRNA which potentially interacts with other vRNAs during selective genome packaging. For this, we used reverse genetics to generate a series of mutant viruses that possessed five silent mutations in either the 3' or 5' packaging signal region of HA vRNA without any amino acid mutations (Fig 1A). The respective viral titers were examined by plaque assays (Fig 1B). Eight out of nine mutant viruses replicated at a level similar to that of the wild-type virus, showing titers of approximately 3.8×10^8 PFU/ml; however, an HA 5m2 virus, possessing five silent mutations at nucleotides 1664 to 1676 in HA vRNA, exhibited an approximately 87% reduced growth rate compared to the wild-type virus. Sequence analysis confirmed that no unexpected mutations occurred in any of the eight vRNAs of the HA 5m2 virus. These results indicate that nucleotides 1664 to 1674 in the packaging signal region of HA vRNA are necessary for efficient virus growth and are likely involved

121 in HA vRNA packaging, which in agreement with results reported by a
122 previous study[14].
123
124 **Serial passaging of the HA 5m2 virus in cells**
125 We hypothesized that after several passages, the HA 5m2 virus
126 would acquire adaptive mutations in vRNAs, which would restore viral
127 fitness. Accordingly, the HA 5m2 virus was serially passaged in Madin-
128 Darby Canine Kidney (MDCK) cells, and viral titers were assessed by
129 plaque assay after each passage. The viruses were designated as HA 5m2
130 P1, P2, P3, P4, P5, P6, P7, P8, P9, and P10 viruses, according to the
131 number of passages in MDCK cells. As expected, the growth of the HA 5m2
132 P10 virus was restored to approximately 61% of that shown by the wild-type
133 virus (Fig 2A). The titer of the HA 5m2 P10 virus did not increase with an
134 additional 10 passages (data not shown). Sequencing analysis of all eight
135 HA 5m2 P10 virus vRNAs revealed that two mutations were newly
136 introduced into the 5' terminal coding regions of HA vRNA (T1665C) and
137 PB2 vRNA (G2271T); both of these vRNAs are located within the previously

identified genome packaging signaling regions [6, 8, 14, 16].

To assess whether these two mutations contributed to the growth of the HA 5m2 virus, we used reverse genetics to generate recombinant HA 5m2 viruses with additional mutation(s). Recombinant HA 5m2 viruses, which possessed a single mutation in HA T1665C or PB2 G2271T, both showed replication that was partially restored to 11 and 24% of the wild-type virus, respectively (Fig 2B). The recombinant HA 5m2 virus with a double mutation showed replication that was approximately 65% of the wild-type virus, similar to the replication levels of the HA 5m2 P10 virus (Fig 2A and 2B).

The HA T1665C and PB2 G2271T mutations lead to amino acid substitutions HA S545P and PB2 Q748H, respectively. The amino acid 545 is located in the transmembrane region of the HA protein; hence, this substitution may affect intracellular transport to the plasma membrane and subsequent incorporation of HA proteins into progeny virions. Therefore, we examined the amount of HA protein incorporated into progeny virions. Western blotting showed that the amounts of HA protein were comparable

155 in the HA 5m2 P10, HA 5m2 P1, and wild-type virions. This suggests that
156 the S545P substitution has little or no effect on the amount of HA protein
157 incorporated into virions (Fig 2C). To examine the impact of the Q748H
158 substitution on the polymerase activity of the PB2 protein, we used RT-
159 qPCR to quantify the amount of vRNA in virus-infected cells at 7 hours post-
160 infection. The amount of vRNA was similar in HA 5m2 P10-infected, HA 5m2
161 P1-infected, and wild-type virus-infected cells, suggesting that the Q748H
162 substitution in PB2 had little or no effect on polymerase activity (Fig 2D).
163 Taken together, these results suggest that T1665C mutations in HA vRNA
164 and G2271T mutations in PB2 vRNA participate in the restoration of HA 5m2
165 viral replication at the RNA level.
166

167 **Efficiency of packaging eight vRNAs in HA 5m2 viruses**

168 Because the HA 5m2 virus possessed five silent mutations in the 5'
169 packaging signal region of HA vRNA, we predicted that it would show
170 defects in the packaging efficiency of vRNAs (especially of HA vRNA). We
171 also expected that additional mutations in the 5' packaging signals of HA

and PB2 vRNAs would improve the packaging efficiency of HA vRNA. To assess the packaging efficiency of the HA 5m2 P1 and HA 5m2 P10 viruses, we extracted vRNA from wild-type, HA 5m2 P1, and HA 5m2 P10 viruses; then, we quantified the amount of the eight influenza vRNA segments using RT-qPCR. As expected, the HA 5m2 P1 virus showed a marked defect in the packaging efficiency of HA vRNA; the packaging efficiency was reduced to approximately 24% compared with that of the wild-type virus. The HA 5m2 P1 virus also showed small defects in the packaging efficiency of PA, NP, and NA vRNAs (Fig 3A). Importantly, in the HA 5m2 P10 virus, the packaging efficiency of HA vRNA was largely recovered to approximately 72% of that in the wild-type, and those of PA, NP, and NA vRNAs were also partially recovered (Fig 3A).

To further examine the contribution of the PB2 G2271T and HA T1665C mutations to vRNA packaging efficiency, we used RT-qPCR to analyze the amount of packaged vRNA in recombinant HA 5m2 viruses possessing a single mutation or a double mutation. In both recombinant HA 5m2 viruses with either a single PB2 G2271T or HA T1665C mutation, the

189 packaging efficiency of HA vRNA was restored to approximately 33 and 59%
190 to that of the wild-type virus, respectively (Fig 3B). In the recombinant HA
191 5m2 virus possessing the double mutation, the packaging efficiency of HA
192 vRNA was largely restored to approximately 77% of that of the wild-type
193 virus (Fig 3B); this was consistent with the packaging efficiency of HA vRNA
194 in the HA 5m2 P10 virus. Taken together, these results show that disruption
195 of the 5' genome packaging signal in HA vRNA reduces the packaging
196 efficiency of HA vRNA. Our results also show that additional mutations in
197 the sequences of 5' genome packaging signals of HA and PB2 vRNAs are
198 required for efficient HA vRNA packaging. This suggests that functional
199 interactions occur between HA and PB2 vRNAs via their 5' genome
200 packaging signals during viral replication.
201
202 **Ultrastructural analysis of the HA 5m2 viruses.**
203 To investigate how the RNPs are packaged into the HA 5m2 P1 and
204 HA 5m2 P10 viruses, we examined ultrathin sections via electron
205 microscopy (EM). Representative images of transversely and longitudinally

206 sectioned wild-type, HA 5m2 P1, and HA 5m2 P10 virions, budding from the
207 cell surfaces, are shown in Fig 4A. While some transversely sectioned wild-
208 type and HA 5m2 P10 virions appeared empty, as reported previously [26],
209 almost all longitudinally sectioned wild-type and HA 5m2 P10 virions
210 contained RNPs positioned at the tip of the budding virions. Conversely, the
211 HA 5m2 P1 viruses often possessed empty particles in both transverse and
212 longitudinal sections, suggesting that the HA 5m2 virus had defects in the
213 incorporation of RNPs.

214 To examine the incorporation of RNPs into virions in more detail,
215 we determined the proportion of empty particles in wild-type, HA 5m2 P1,
216 and HA 5m2 P10 viruses. For this, virions were purified by
217 ultracentrifugation through a sucrose cushion and observed by cryo-TEM
218 (Fig 4B). The particles of the wild-type virus mainly showed uniformly
219 spherical shapes of approximately 111 nm in diameter; 0.9% (n=1085) of
220 virions appeared empty or contained only a few vRNPs (Table 1). With a
221 diameter of approximately 87 nm (n=10, $p<0.0001$), such vRNP packaging-
222 deficient particles were significantly smaller than intact virions containing

multiple RNPs. The proportion of vRNP packaging-deficient particles in the HA 5m2 P1 virus was 7.0% (n=1401), significantly higher than those of the HA 5m2 P10 (3.2%, n=852, $p<0.0001$) and wild-type (0.9%, n=1085, $p<0.0001$) viruses. The results of EM analysis support the notion that potential interactions between the 5' packaging signals of HA and PB2 vRNAs are important for appropriate genome packaging.

Table 1. Effect of silent mutations and passages on the packaging of RNPs into progeny virions

	Experiment no.	wt	HA 5m2 P1	HA 5m2 P10
Proportion of vRNP packaging-deficient particles	1	3 / 341 (0.9%)	32 / 505 (6.3%)	14 / 370 (3.7%)
	2	7 / 744 (0.9%)	66 / 896 (7.4%)	13 / 482 (2.7%)
	Total	10 / 1085 (0.9%)	98 / 1401 (7.0%)	27 / 852 (3.2%)
p-value*		<0.0001		<0.0001

*Proportions of vRNP packaging-deficient particles in each virus were compared with that in the HA 5m2 P1 virus. Data were analyzed using Dunnett's test.

A direct interaction between HA and PB2 vRNA occurs via the 5' ends of packaging signals *in vitro*

We next aimed to confirm that a functional interaction between the 5' terminal regions of HA and PB2 vRNAs is involved in efficient packaging of HA vRNA. For this, we used a gel shift assay to examine whether direct RNA-RNA interactions between these two vRNAs occur *in vitro*. To eliminate possible nonspecific interactions via the non-packaging signal regions of vRNAs, we synthesized a short HA vRNA comprising the 5' noncoding region and the 120-nucleotide long coding region, which is designated as 5'HA(120). We also synthesized a short PB2 vRNA comprising the 5' noncoding region and the 300-nucleotide long coding region, which is designated as 5'PB2(300) (Fig 5A). In addition to the 5'HA(120) possessing the wild-type HA vRNA sequence, we synthesized mutant 5'HA(120) sequences into which we introduced five silent mutations corresponding to HA 5m1, HA 5m2, HA 5m3, HA 5m4, and HA 5m5 (Fig 1A); these mutant 5'HA(120) vRNAs were designated as 5'HA(120) 5m1, 5'HA(120) 5m2, 5'HA(120) 5m3, 5'HA(120) 5m4, and 5'HA(120) 5m5, respectively. The

mixture of wild-type 5'HA(120) and 5'PB2(300) showed slower migration of the band, indicating formation of a vRNA-vRNA complex (Figs 5B and 5C). The mutant 5'HA(120) 5m1, 5'HA(120) 5m3, 5'HA(120) 5m4, and 5'HA(120) 5m5 vRNAs also formed a complex with 5'PB2(300), whose proportions were 69-95% compared to the complex of 5'HA(120) and 5'PB2(300). These results are consistent with our viral replication data, showing that such mutations in HA vRNA did not markedly affect viral growth (Fig 1B). In contrast, the 5'HA(120) 5m2 vRNA associated with 5'PB2(300) to a lesser degree and did not form a vRNA-vRNA complex efficiently, with only 12% complex formation compared to the 5'HA(120) and 5'PB2(300), correlating with the reduced viral growth of the HA 5m2 virus (Fig 1B). Taken together, these results indicate that there is an interaction between the 5' packaging signals of HA and PB2 vRNAs in the context of vRNPs, which is important for optimal packaging of HA vRNA.

Discussion

Specific interactions among eight different vRNAs are likely required for selective genome packaging of the influenza viruses. To identify the interactions of HA vRNA in the context of RNPs, we generated a mutant HA 5m2 virus with reduced packaging efficiency of HA vRNA, and repeatedly passaged this virus in cultured cells to restore viral fitness. We found that the HA 5m2 virus acquired additional mutations in the 5’ packaging signal sequences of HA and PB2 vRNAs; this restored HA vRNA packaging efficiency and viral growth. Our results suggest that the packaging signal at the 5' terminal coding region of HA vRNA is involved in co-packaging of the eight different vRNAs; this likely occurs via a direct RNA-RNA interaction with the 5’ packaging signal of PB2 vRNA. To the best of our knowledge, this is the first study experimentally showing that a packaging-deficient virus can recover its packaging efficiency by the introduction of mutations in other vRNA segments during viral replication.

The 5’ packaging signal sequence, located at nucleotides 1662 to 1681 in HA vRNA, is more than 90% conserved in H1 subtype influenza

283 viruses. However, the neighboring regions show less sequence
284 conservation [14], suggesting that this region is important for HA vRNA
285 packaging at the RNA level. Our results show that introduction of five silent
286 mutations into the highly conserved region at nucleotides 1664 to 1676 in
287 HA vRNA reduced the incorporation efficiency of HA vRNA (Fig. 2A). An
288 additional mutation at nucleotide 1665 restored the reduced efficiency of
289 HA vRNA packaging (Fig. 2B). This confirms that the highly conserved
290 region in the sequence of the 5' terminal packaging signal is involved in
291 incorporation of HA vRNA. Recent findings indicate that NP non-uniformly
292 decorates vRNA [1, 2]. Therefore, it is possible that the region at
293 nucleotides 1664 to 1676 in HA vRNA, identified in this study, is NP-free
294 and forms secondary or tertiary structures on vRNPs to interact with the 5'
295 packaging signal of PB2 vRNA. However, whether the 5' terminal coding
296 region of HA vRNA is a low NP-binding region remains unclear [1, 2].
297 Additional work is necessary to determine the precise location of the NP-
298 free region of HA vRNA in the A/WSN/33 strain.

299 After the HA 5m2 virus was serially passaged in MDCK cells, the

virus acquired a G2271T mutation in the 5’ packaging signal sequence of PB2 vRNA, which recovered the reduced incorporation of HA vRNA (Fig. 2B). This finding suggests that the region around nucleotide 2271 in PB2 vRNA is involved in interactions with HA vRNA. However, a previous study showed that the introduction of silent mutations at nucleotides 2268 to 2286, including a mutation at nucleotide 2271, in PB2 vRNA did not reduce the packaging efficiency of HA vRNA [14]. Therefore, it is possible that the mutation at G2271T in PB2 vRNA, found in this study, was acquired for the optimal packaging of HA 5m2 vRNA but not of wild-type HA vRNA.

Although the 5' terminal coding region of H1 subtype HA vRNA is conserved in H1 HA vRNA, it is substantially different from other subtypes of HA vRNAs at the nucleotide level [13]. In contrast, the 5’ terminal coding region of PB2 vRNA is highly conserved in influenza viruses [13, 17], suggesting that intersegmental interactions between HA and PB2 vRNAs via their 5’ terminal regions may be specific to the H1 subtype. Native gel electrophoresis analysis of *in-vitro* vRNA-vRNA interactions revealed that avian H5N2 and human H3N2 viruses show different intersegmental

317 networks among the eight vRNAs, and do not show strong interactions
318 between HA and PB2 vRNAs [22, 24]. In the context of vRNPs, *in-vitro*
319 interactions do not necessarily reflect interactions *in-vivo*. Therefore,
320 further studies are needed to clarify whether HA vRNAs of other subtypes
321 require interactions with PB2 vRNA for HA vRNA packaging in the context
322 of vRNPs.

323 The reduced HA vRNA packaging efficiency of the HA 5m2 virus was
324 rescued when the virus spontaneously acquired adaptive mutations in HA
325 and PB2 vRNAs during serial passaging (Fig. 2A and 2B). Previously, Marsh
326 et al., serially passaged an influenza A virus (WSN strain), which possesses
327 synonymous mutations in HA vRNAs, to determine whether the virus would
328 generate adaptive mutations for recovery of the reduced HA vRNA
329 packaging efficiency. However, the virus did not generate any mutations to
330 improve viral fitness [14]. This may have been due to the number of
331 synonymous mutations introduced into the HA vRNAs. Nine nucleotide
332 mutations were introduced into the region of 1659 to 1673 in the HA vRNAs
333 in the study by Marsh et al., while only five mutations were introduced into

334 the region of 1664 to 1679 in HA vRNAs in our present study. More
335 mutations may cause severe incompatibility in vRNA-vRNA interactions.
336 Even repeated serial passaging may not generate multiple nucleotide
337 changes in HA vRNA and its respective interacting vRNA to restore the HA
338 vRNA packaging efficiency.

339 In conclusion, we have shown that an interaction between HA vRNA
340 and PB2 vRNA via the 5' packaging signals is important for HA vRNA
341 packaging. Our results suggest that HA vRNA is co-packaged with PB2
342 vRNA into virions. These findings will help us understand how reassortant
343 influenza viruses incorporate HA vRNA segments, and how pandemic
344 viruses emerge via genetic reassortment.
345

Materials and Methods

Cells

Human embryonic kidney (293T) cells were maintained in Dulbecco's Modified Eagle Medium (D6046, Sigma) supplemented with 10% fetal bovine serum (FB-1365, Biosera, Chile). Madin-Darby Canine Kidney (MDCK) cells were grown in Minimal Essential Medium (MEM)(11430-030, Gibco) containing 5% newborn calf serum (16010-159, Gibco, New Zealand). Cultures were maintained at 37˚C in a 5% CO_2 atmosphere. The medium used during viral infection of cells was MEM containing 0.3% bovine serum albumin (BSA/MEM).

Construction of the PolI HA plasmid

To generate the PolI HA mutant plasmid, we amplified the PolI-HA plasmid by inverse PCR using a previously published protocol [27]. The primers used are listed in S1 Table.

Reverse genetics

Reverse genetics were performed using PolI plasmids that contained cDNA sequences of the A/WSN/33(H1N1) viral genes; all procedures were conducted as described previously [28]. Briefly, eight PolI plasmids and pCAGGS protein-expression plasmids for PB2, PB1, PA, and NP were mixed with the transfection reagent TransIT-293 (Mirus), and added to 293T cells cultured in BSA/MEM. At 48 hours post-transfection, the cells were treated with 1 μg /ml of TPCK-Trypsin for 30 min, centrifuged at 1750 × g for 15 min at 4ºC, and the supernatant was harvested and stored at -80ºC. To generate mutant viruses, the PolI-HA wt plasmid was replaced with a PolI-HA mutant plasmid. Viral titers were determined by a plaque assay conducted using MDCK cells.

Virus purification

After collecting the supernatants from virus-infected MDCK cells, each supernatant was clarified by centrifugation at 1750 × g for 15 min at 4ºC, followed by another centrifugation at 6700 × g for 30 min at 4ºC. To eliminate RNAs outside of the virus particles, the supernatants were treated

with 5 μg/ml RNase A (Nacalai Tesque) for 1 hour at 37°C. Virions in the supernatants were purified by ultracentrifugation through a 30% (w/w) sucrose cushion at 125,000 × g for 2 hours at 4°C. The pellets were then resuspended in phosphate buffered saline (PBS).

Western blotting

MDCK cells were infected with the viruses at a multiplicity of infection (MOI) of 1 on ice for 1 hour. The infected MDCK cells were then cultured in BSA/MEM containing 1 μg /ml TPCK-Trypsin. At 10 hours post-infection, the supernatant was harvested and purified as described above. The purified virus was dissolved with an equal volume of 2x Tris-Glycine SDS Sample Buffer (Thermo Fisher Scientific) and boiled for 5 min without a reducing agent, and then subjected to SDS-PAGE. Proteins were electroblotted onto Immobilon-P transfer membranes (Millipore Corporation). The membranes were blocked with Blocking One (Nacalai Tesque) for 30 min at room temperature, and then incubated with goat anti-influenza A virus polyclonal antibody (ab20841, Abcam, 1:10,000 dilution)

overnight at 4°C. After incubation with rabbit anti-goat IgG secondary antibody (ab6741, Abcam, 1:10,000 dilution) for 1 hour at room temperature, the blots were developed using a Chemi-Lumi One Super (Nacalai Tesque).

RT-qPCR

The packaged vRNAs were extracted from purified viruses using an RNeasy Mini Kit (Qiagen). 100 ng of extracted vRNAs were reverse transcribed using a Uni-12 primer (5'-AGCRAAAGCAGG-3') and Superscript III reverse transcriptase (Invitrogen). Quantification was performed by qPCR on a Rotor-Gene Q 2plex System (Qiagen) using segment-specific primers modified from the protocol by Marsh *et al*. The primers used are listed in S1 Table. For each sample, reactions contained 1 µl 10-fold diluted RT product, 7.5 µl THUNDERBIRD SYBR qPCR Mix (Toyobo), 0.25 µM segment-specific primers, for a final volume of 15 µl. Cycling conditions were: 2 min at 94°C, followed by 40 cycles (98°C for 10 s, 55°C for 15 s, and 72°C for 30 s).

In Figure 2D, total RNA was extracted from virus-infected cells

414 using an RNeasy Mini Kit (Qiagen). For PB2, PB1, HA, and NP vRNAs, RT-
415 qPCR was performed as described above, using 100 ng total RNA. The
416 values were expressed as numbers of RNA copies in an infected cell,
417 assuming that a cell contained 10 pg of RNA [29, 30].
418
419 **Ultrathin section electron microscopy (EM)**
420 Ultrathin section EM was performed as described previously [3].
421 MDCK cells were infected at MOI=10. At 10 hours post-infection, the
422 infected cells were prefixed with 2.5% glutaraldehyde in 0.1 M cacodylate
423 buffer (pH 7.4) on ice. Ultrathin (50-nm-thick) sections were stained with 2%
424 uranyl acetate in 70% ethanol and in Reynold's lead citrate. Representative
425 images were acquired using HT7700 (Hitachi).
426
427 **Quantification of vRNP packaging-deficient particles**
428 Purified viruses were applied onto C-flat holey carbon grids
429 (Protichips), which were blotted on a Vitrobot Mark IV (Thermo Fisher
430 Scientific) before plunge-freezing in liquid ethane. Samples were kept cool

in liquid nitrogen. Samples were imaged at 200 kV on a Talos F200C (Thermo Fisher Scientific) equipped with a Ceta 16M CMOS camera (Gatan). More than 300 particles were observed for each experiment.

In vitro RNA synthesis

Shortened HA and PB2 vRNAs were synthesized *in vitro* using T7 transcription as described previously [30]. Briefly, templates containing a T7 phage promoter sequence (5'-TAATACGACTCACTATAGGG-3') were amplified by PCR using corresponding primer pairs and were purified with a QIAquick PCR purification kit (Qiagen). The primers used are listed in S1 Table. Purified PCR products were transcribed *in vitro* using the RiboMAX Large Scale RNA Production System-T7 (Promega) at 37°C for 4 h, followed by RQ1 DNase I (Promega) digestion of the DNA template at 37°C for 15 min. The transcript was purified with an RNeasy Mini Kit.

RNA binding assay

RNA-RNA interactions were analyzed by electrophoretic mobility

448 shift assays essentially as described previously [24]. To facilitate RNA
449 folding, adjustments were made to the reaction buffer employed and
450 incubation time as described below [31]. Pairs of purified vRNAs (2 pmol of
451 each vRNA) were denatured for 10 min at 65°C in 5 µl of ultrapure water
452 and cooled on ice. We then added 5 µl of 2-fold concentrated buffer (final
453 concentration: 50 mM HEPES, 50 mM KCl, and 20 mM $MgCl_2$) and incubated
454 the samples for 2 hours at 37°C. Then, 2 µl of loading buffer [40% (v/v)
455 glycerol and 0.05% (w/v) bromophenol blue] was added to the samples, and
456 the samples were analyzed using 1.0% agarose gels containing 0.01% (w/v)
457 ethidium bromide. Native gel electrophoresis of the RNA complexes was
458 performed at 4°C in a buffer containing 50 mM Tris, 44.5 mM borate, and
459 0.1 mM $MgCl_2$. We then determined the RNA weight fraction (%) of each
460 band in each lane. The percentage of intermolecular complex formation was
461 determined by dividing the weight fraction of a band by the sum of weight
462 fractions in the corresponding lane.
463

464 **Statistical analysis**

The statistical significance of the viral titers, the proportions of vRNP packaging-deficient particles and the formation efficiencies of vRNA-vRNA complexes were calculated using Dunnett's test. Diameters of virus particles observed by EM were statistically analyzed using Welch's t-test. P values of < 0.01 were considered significant.

Acknowledgments

We thank Connor Park for editing the manuscript.

References

1. Williams GD, Townsend D, Wylie KM, Kim PJ, Amarasinghe GK, Kutluay SB, et al. Nucleotide resolution mapping of influenza A virus nucleoprotein-RNA interactions reveals RNA features required for replication. Nature communications. 2018;9(1):465. Epub 2018/02/02. doi: 10.1038/s41467-018-02886-w. PubMed PMID: 29386621; PubMed Central PMCID: PMCPMC5792457.

2. Lee N, Le Sage V, Nanni AV, Snyder DJ, Cooper VS, Lakdawala SS. Genome-wide analysis of influenza viral RNA and nucleoprotein association. Nucleic acids research. 2017;45(15):8968-77. doi: 10.1093/nar/gkx584.

3. Noda T, Sagara H, Yen A, Takada A, Kida H, Cheng RH, et al. Architecture of ribonucleoprotein complexes in influenza A virus particles. Nature. 2006;439(7075):490-2. Epub 2006/01/27. doi: 10.1038/nature04378. PubMed PMID: 16437116.

4. Chou YY, Vafabakhsh R, Doganay S, Gao Q, Ha T, Palese P. One influenza virus particle packages eight unique viral RNAs as shown by FISH analysis. Proceedings of the National Academy of Sciences of the United

491 States of America. 2012;109(23):9101-6. Epub 2012/05/02. doi:
492 10.1073/pnas.1206069109. PubMed PMID: 22547828; PubMed Central
493 PMCID: PMCPMC3384215.
494 5. Fujii Y, Goto H, Watanabe T, Yoshida T, Kawaoka Y. Selective
495 incorporation of influenza virus RNA segments into virions. Proceedings of
496 the National Academy of Sciences of the United States of America.
497 2003;100(4):2002-7. Epub 2003/02/08. doi: 10.1073/pnas.0437772100.
498 PubMed PMID: 12574509; PubMed Central PMCID: PMCPMC149948.
499 6. Watanabe T, Watanabe S, Noda T, Fujii Y, Kawaoka Y. Exploitation
500 of nucleic acid packaging signals to generate a novel influenza virus-based
501 vector stably expressing two foreign genes. Journal of virology.
502 2003;77(19):10575-83. Epub 2003/09/13. PubMed PMID: 12970442;
503 PubMed Central PMCID: PMCPMC228515.
504 7. Fujii K, Fujii Y, Noda T, Muramoto Y, Watanabe T, Takada A, et al.
505 Importance of both the coding and the segment-specific noncoding regions
506 of the influenza A virus NS segment for its efficient incorporation into virions.
507 Journal of virology. 2005;79(6):3766-74. Epub 2005/02/26. doi:

508 10.1128/jvi.79.6.3766-3774.2005. PubMed PMID: 15731270; PubMed
509 Central PMCID: PMCPMC1075679.
510 8. Muramoto Y, Takada A, Fujii K, Noda T, Iwatsuki-Horimoto K,
511 Watanabe S, et al. Hierarchy among viral RNA (vRNA) segments in their
512 role in vRNA incorporation into influenza A virions. Journal of virology.
513 2006;80(5):2318-25. Epub 2006/02/14. doi: 10.1128/jvi.80.5.2318-
514 2325.2006. PubMed PMID: 16474138; PubMed Central PMCID:
515 PMCPMC1395381.
516 9. Ozawa M, Fujii K, Muramoto Y, Yamada S, Yamayoshi S, Takada A,
517 et al. Contributions of two nuclear localization signals of influenza A virus
518 nucleoprotein to viral replication. Journal of virology. 2007;81(1):30-41.
519 Epub 2006/10/20. doi: 10.1128/jvi.01434-06. PubMed PMID: 17050598;
520 PubMed Central PMCID: PMCPMC1797272.
521 10. Ozawa M, Maeda J, Iwatsuki-Horimoto K, Watanabe S, Goto H,
522 Horimoto T, et al. Nucleotide sequence requirements at the 5' end of the
523 influenza A virus M RNA segment for efficient virus replication. Journal of
524 virology. 2009;83(7):3384-8. Epub 2009/01/23. doi: 10.1128/jvi.02513-08.

525 PubMed PMID: 19158245; PubMed Central PMCID: PMCPMC2655591.

526 11. Goto H, Muramoto Y, Noda T, Kawaoka Y. The genome-packaging
527 signal of the influenza A virus genome comprises a genome incorporation
528 signal and a genome-bundling signal. Journal of virology.
529 2013;87(21):11316-22. Epub 2013/08/09. doi: 10.1128/jvi.01301-13.
530 PubMed PMID: 23926345; PubMed Central PMCID: PMCPMC3807325.

531 12. Liang Y, Hong Y, Parslow TG. cis-Acting packaging signals in the
532 influenza virus PB1, PB2, and PA genomic RNA segments. Journal of
533 virology. 2005;79(16):10348-55. Epub 2005/07/30. doi:
534 10.1128/jvi.79.16.10348-10355.2005. PubMed PMID: 16051827; PubMed
535 Central PMCID: PMCPMC1182667.

536 13. Gog JR, Afonso Edos S, Dalton RM, Leclercq I, Tiley L, Elton D, et
537 al. Codon conservation in the influenza A virus genome defines RNA
538 packaging signals. Nucleic acids research. 2007;35(6):1897-907. Epub
539 2007/03/03. doi: 10.1093/nar/gkm087. PubMed PMID: 17332012; PubMed
540 Central PMCID: PMCPMC1874621.

541 14. Marsh GA, Hatami R, Palese P. Specific residues of the influenza A

542 virus hemagglutinin viral RNA are important for efficient packaging into
543 budding virions. Journal of virology. 2007;81(18):9727-36. Epub 2007/07/20.
544 doi: 10.1128/jvi.01144-07. PubMed PMID: 17634232; PubMed Central
545 PMCID: PMCPMC2045411.
546 15. Hutchinson EC, Curran MD, Read EK, Gog JR, Digard P. Mutational
547 analysis of cis-acting RNA signals in segment 7 of influenza A virus. Journal
548 of virology. 2008;82(23):11869-79. Epub 2008/09/26. doi:
549 10.1128/jvi.01634-08. PubMed PMID: 18815307; PubMed Central PMCID:
550 PMCPMC2583641.
551 16. Liang Y, Huang T, Ly H, Parslow TG, Liang Y. Mutational analyses
552 of packaging signals in influenza virus PA, PB1, and PB2 genomic RNA
553 segments. Journal of virology. 2008;82(1):229-36. Epub 2007/10/26. doi:
554 10.1128/jvi.01541-07. PubMed PMID: 17959657; PubMed Central PMCID:
555 PMCPMC2224372.
556 17. Marsh GA, Rabadan R, Levine AJ, Palese P. Highly conserved
557 regions of influenza a virus polymerase gene segments are critical for
558 efficient viral RNA packaging. Journal of virology. 2008;82(5):2295-304.

559 Epub 2007/12/21. doi: 10.1128/jvi.02267-07. PubMed PMID: 18094182;
560 PubMed Central PMCID: PMCPMC2258914.
561 18. Hutchinson EC, Wise HM, Kudryavtseva K, Curran MD, Digard P.
562 Characterisation of influenza A viruses with mutations in segment 5
563 packaging signals. Vaccine. 2009;27(45):6270-5. Epub 2009/10/21. doi:
564 10.1016/j.vaccine.2009.05.053. PubMed PMID: 19840659; PubMed Central
565 PMCID: PMCPMC2771075.
566 19. Gao Q, Chou YY, Doganay S, Vafabakhsh R, Ha T, Palese P. The
567 influenza A virus PB2, PA, NP, and M segments play a pivotal role during
568 genome packaging. Journal of virology. 2012;86(13):7043-51. Epub
569 2012/04/26. doi: 10.1128/jvi.00662-12. PubMed PMID: 22532680; PubMed
570 Central PMCID: PMCPMC3416350.
571 20. Chou YY, Heaton NS, Gao Q, Palese P, Singer RH, Lionnet T.
572 Colocalization of different influenza viral RNA segments in the cytoplasm
573 before viral budding as shown by single-molecule sensitivity FISH analysis.
574 PLoS pathogens. 2013;9(5):e1003358. Epub 2013/05/15. doi:
575 10.1371/journal.ppat.1003358. PubMed PMID: 23671419; PubMed Central

576 PMCID: PMCPMC3649991.

577 21. Lakdawala SS, Wu Y, Wawrzusin P, Kabat J, Broadbent AJ,
578 Lamirande EW, et al. Influenza a virus assembly intermediates fuse in the
579 cytoplasm. PLoS pathogens. 2014;10(3):e1003971. Epub 2014/03/08. doi:
580 10.1371/journal.ppat.1003971. PubMed PMID: 24603687; PubMed Central
581 PMCID: PMCPMC3946384.

582 22. Fournier E, Moules V, Essere B, Paillart JC, Sirbat JD, Isel C, et al.
583 A supramolecular assembly formed by influenza A virus genomic RNA
584 segments. Nucleic acids research. 2012;40(5):2197-209. Epub 2011/11/15.
585 doi: 10.1093/nar/gkr985. PubMed PMID: 22075989; PubMed Central
586 PMCID: PMCPMC3300030.

587 23. Noda T, Sugita Y, Aoyama K, Hirase A, Kawakami E, Miyazawa A,
588 et al. Three-dimensional analysis of ribonucleoprotein complexes in
589 influenza A virus. Nature communications. 2012;3:639. Epub 2012/01/26.
590 doi: 10.1038/ncomms1647. PubMed PMID: 22273677; PubMed Central
591 PMCID: PMCPMC3272569.

592 24. Gavazzi C, Isel C, Fournier E, Moules V, Cavalier A, Thomas D, et

593 al. An in vitro network of intermolecular interactions between viral RNA
594 segments of an avian H5N2 influenza A virus: comparison with a human
595 H3N2 virus. Nucleic acids research. 2013;41(2):1241-54. Epub 2012/12/12.
596 doi: 10.1093/nar/gks1181. PubMed PMID: 23221636; PubMed Central
597 PMCID: PMCPMC3553942.
598 25. Gilbertson B, Zheng T, Gerber M, Printz-Schweigert A, Ong C,
599 Marquet R, et al. Influenza NA and PB1 Gene Segments Interact during the
600 Formation of Viral Progeny: Localization of the Binding Region within the
601 PB1 Gene. Viruses. 2016;8(8). Epub 2016/08/25. doi: 10.3390/v8080238.
602 PubMed PMID: 27556479; PubMed Central PMCID: PMCPMC4997600.
603 26. Gavazzi C, Yver M, Isel C, Smyth RP, Rosa-Calatrava M, Lina B, et
604 al. A functional sequence-specific interaction between influenza A virus
605 genomic RNA segments. Proceedings of the National Academy of Sciences
606 of the United States of America. 2013;110(41):16604-9. Epub 2013/09/27.
607 doi: 10.1073/pnas.1314419110. PubMed PMID: 24067651; PubMed Central
608 PMCID: PMCPMC3799358.
609 27. Ochman H, Gerber AS, Hartl DL. Genetic applications of an inverse

610 polymerase chain reaction. Genetics. 1988;120(3):621-3. Epub 1988/11/01.

611 PubMed PMID: 2852134; PubMed Central PMCID: PMCPMC1203539.

612 28. Neumann G, Watanabe T, Ito H, Watanabe S, Goto H, Gao P, et al.

613 Generation of influenza A viruses entirely from cloned cDNAs. Proceedings

614 of the National Academy of Sciences of the United States of America.

615 1999;96(16):9345-50. Epub 1999/08/04. PubMed PMID: 10430945; PubMed

616 Central PMCID: PMCPMC17785.

617 29. Hatada E, Hasegawa M, Mukaigawa J, Shimizu K, Fukuda R.

618 Control of Influenza Virus Gene Expression: Quantitative Analysis of Each

619 Viral RNA Species in Infected Cells. The Journal of Biochemistry.

620 1989;105(4):537-46.

621 30. Kawakami E, Watanabe T, Fujii K, Goto H, Watanabe S, Noda T, et

622 al. Strand-specific real-time RT-PCR for distinguishing influenza vRNA,

623 cRNA, and mRNA. Journal of virological methods. 2011;173(1):1-6. Epub

624 2010/12/28. doi: 10.1016/j.jviromet.2010.12.014. PubMed PMID: 21185869;

625 PubMed Central PMCID: PMCPMC3049850.

626 31. Buchmueller KL, Weeks KM. Tris-borate is a poor counterion for

627 RNA: a cautionary tale for RNA folding studies. Nucleic acids research.

628 2004;32(22):e184. Epub 2004/12/17. doi: 10.1093/nar/gnh182. PubMed

629 PMID: 15601995; PubMed Central PMCID: PMCPMC545480.

630

A.

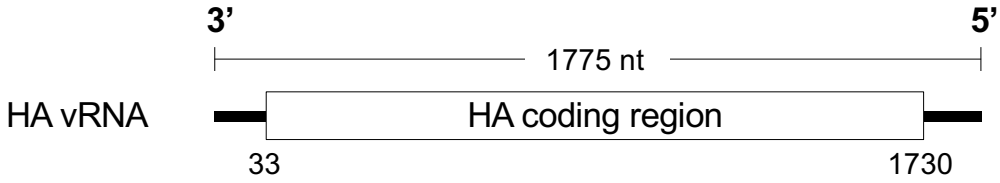


```
                33       40                          60                          80                          98
HA wt           ATG AAG GCA AAA CTA CTG GTC CTG TTA TAT GCA TTT GTA GCT ACA GAT GCA GAC ACA ATA TGT ATA
HA 3m1          ... ... ..G ..G ..G ..A ..A ... ... ... ... ... ... ... ... ... ... ... ... ... ... ...
HA 3m2          ... ... ... ... ... ... ... ..A ..G ..C ..G ..C ... ... ... ... ... ... ... ... ... ...
HA 3m3          ... ... ... ... ... ... ... ... ... ... ... ... ..T ..A ..C ..C ..T ... ... ... ... ...
HA 3m4          ... ... ... ... ... ... ... ... ... ... ... ... ... ... ... ... ... ... ..T ..C ..C ..C ..C

                1647            1660                        1680                        1700            1712
HA wt           TCA CTG GTG CTT TTG GTC TCC CTG GGG GCA ATC AGT TTC TGG ATG TGT TCT AAT GGG TCT TTG CAG
HA 5m1          ..C ..A ..C ..G ..A ... ... ... ... ... ... ... ... ... ... ... ... ... ... ... ... ...
HA 5m2          ... ... ... ... ... ..A ..A ..A ..A ..C ... ... ... ... ... ... ... ... ... ... ... ...
HA 5m3          ... ... ... ... ... ... ... ... ... ... ..A ..C ..T ... ... ..C ..C ... ... ... ... ...
HA 5m4          ... ... ... ... ... ... ... ... ... ... ... ... ... ... ... ... ... ... ..C ..A ..A ..A ..A

                1713    1720        1730
HA wt           TGC AGA ATA TGC ATC TGA
HA 5m5          ..T ..G ..C ..T ..T ...
```

B.

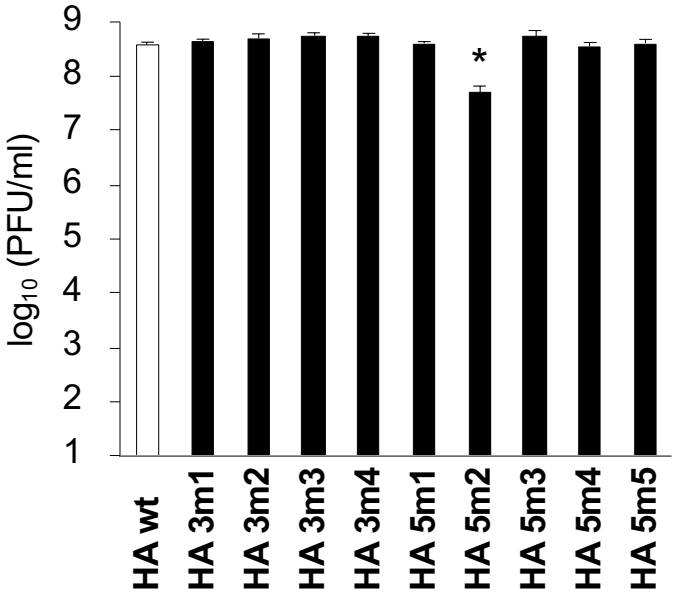

Fig 1. Generation of mutant influenza A viruses by reverse genetics and replication efficiencies of these mutant viruses. (A) Schematic diagram of mutant HA vRNAs with silent mutations introduced into the packaging signal sequences. The 3' and 5' ends of the HA coding region (nucleotides 33–98 and 1649–1730, respectively) are shown in the mRNA-sense orientation. (B) 293T cells were transfected with plasmids to produce the mutant and wild-type viruses. MDCK cells were infected with these mutant and wild-type viruses at a multiplicity of infection (MOI) of 10^{-5}. Virus yields at 48 h post-infection were determined by a plaque assay on MDCK cells. The data represent the mean ± SD (n = 3). Dunnett's test; *P < 0.01

Figure 1

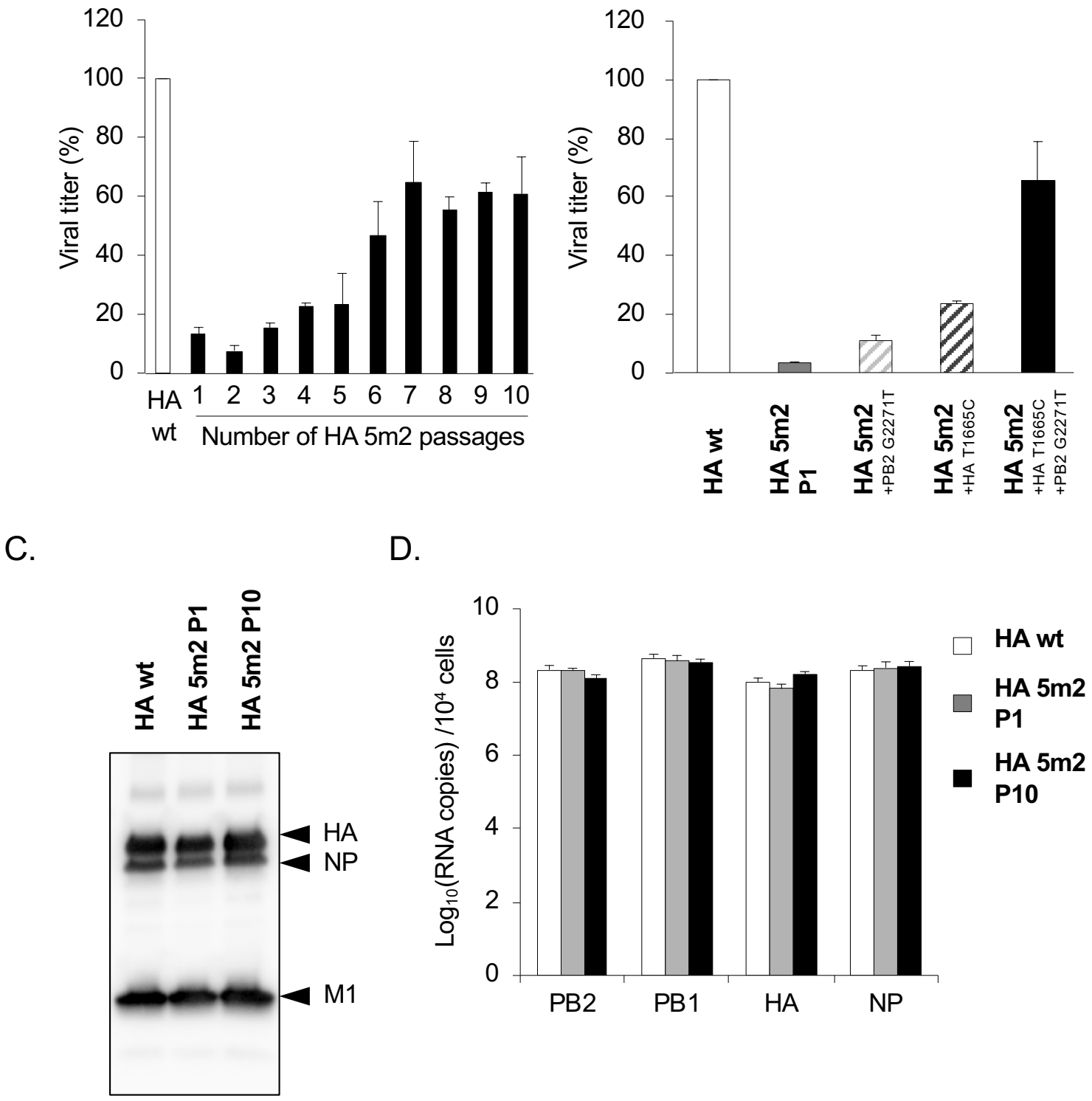

Fig 2. Analysis of HA 5m2 viral replication. (A) The HA 5m2 virus was passaged in MDCK cells at an MOI of 10^{-5}. For each passage, supernatants were collected at 48 hours post-infection, and viral yields were determined by a plaque assay on MDCK cells. (B) 293T cells were transfected with plasmids to produce the mutant HA5m2 and wild-type viruses. After infecting MDCK cells at an MOI of 10^{-5}, viral yields were determined at 48 hours post-infection. The data represent the mean ± SD (n = 3). (C) The purified viruses were analyzed via western blot using an anti-influenza A virus polyclonal antibody against HA, NP, and M1. (D) MDCK cells were infected with the viruses at an MOI of 1. Total RNA was extracted at 7 hours post-infection. PB2, PB1, HA, and NP vRNAs were analyzed using RT-qPCR analysis. Data represent the mean ±SD of two independent experiments, each performed in triplicate.

Figure 2

A.

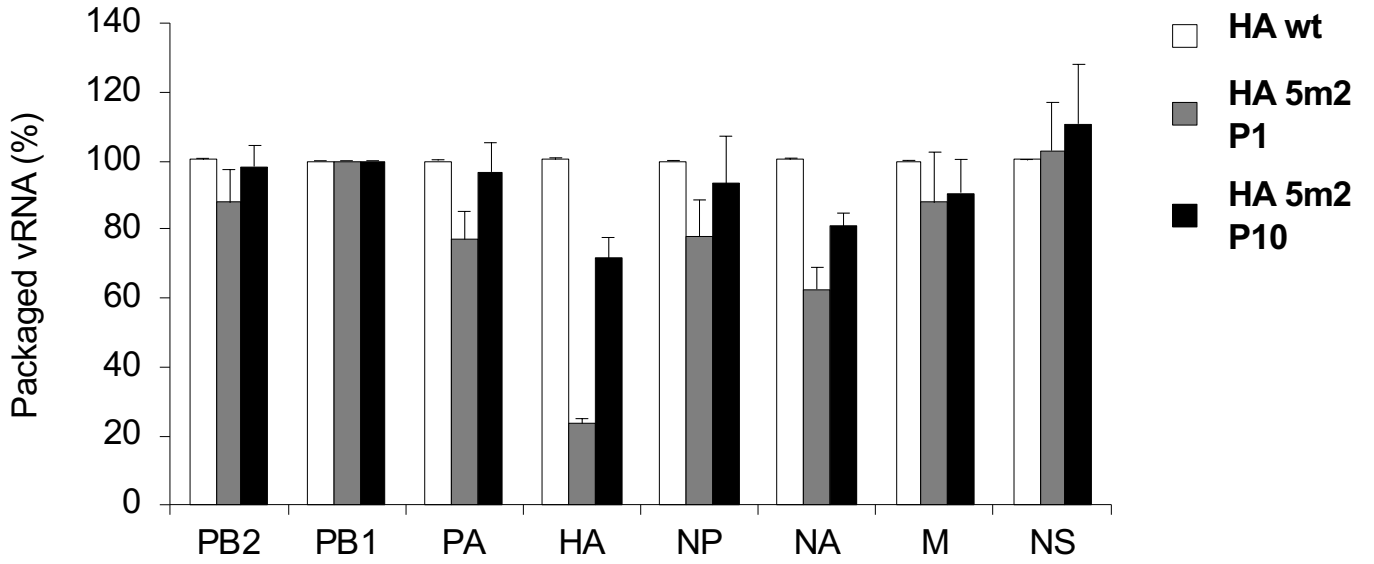

B.

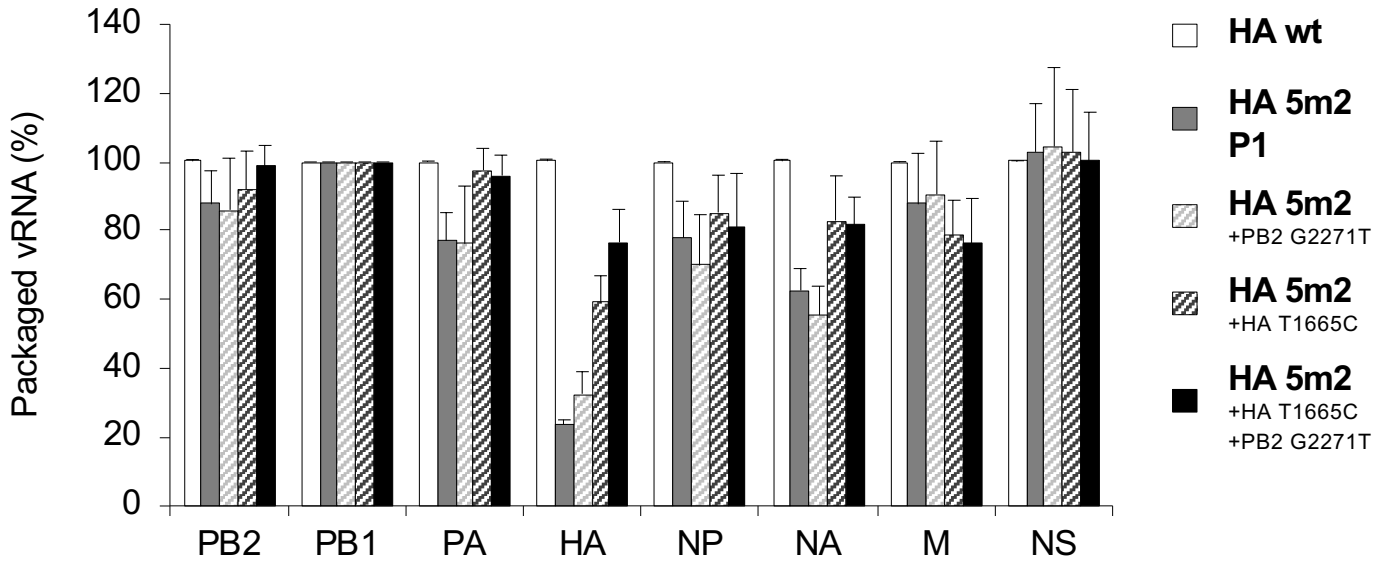

Fig 3. **Packaging of individual vRNA segments into progeny viral particles.** The amount of vRNA extracted from purified virus particles was quantified by RT-qPCR. All vRNAs were normalized to the amount of PB1 vRNA and to the average of that contained in the wild-type virus. Data represent the mean ±SD from two independent experiments each conducted in triplicate. (A) The panel shows the relative amounts of eight vRNA from the wild-type virus, HA 5m2 P10 virus, and HA 5m2 P1 virus. (B) The panel shows the relative amounts of eight vRNA from the wild-type virus and mutant HA 5m2 viruses.

Figure 3

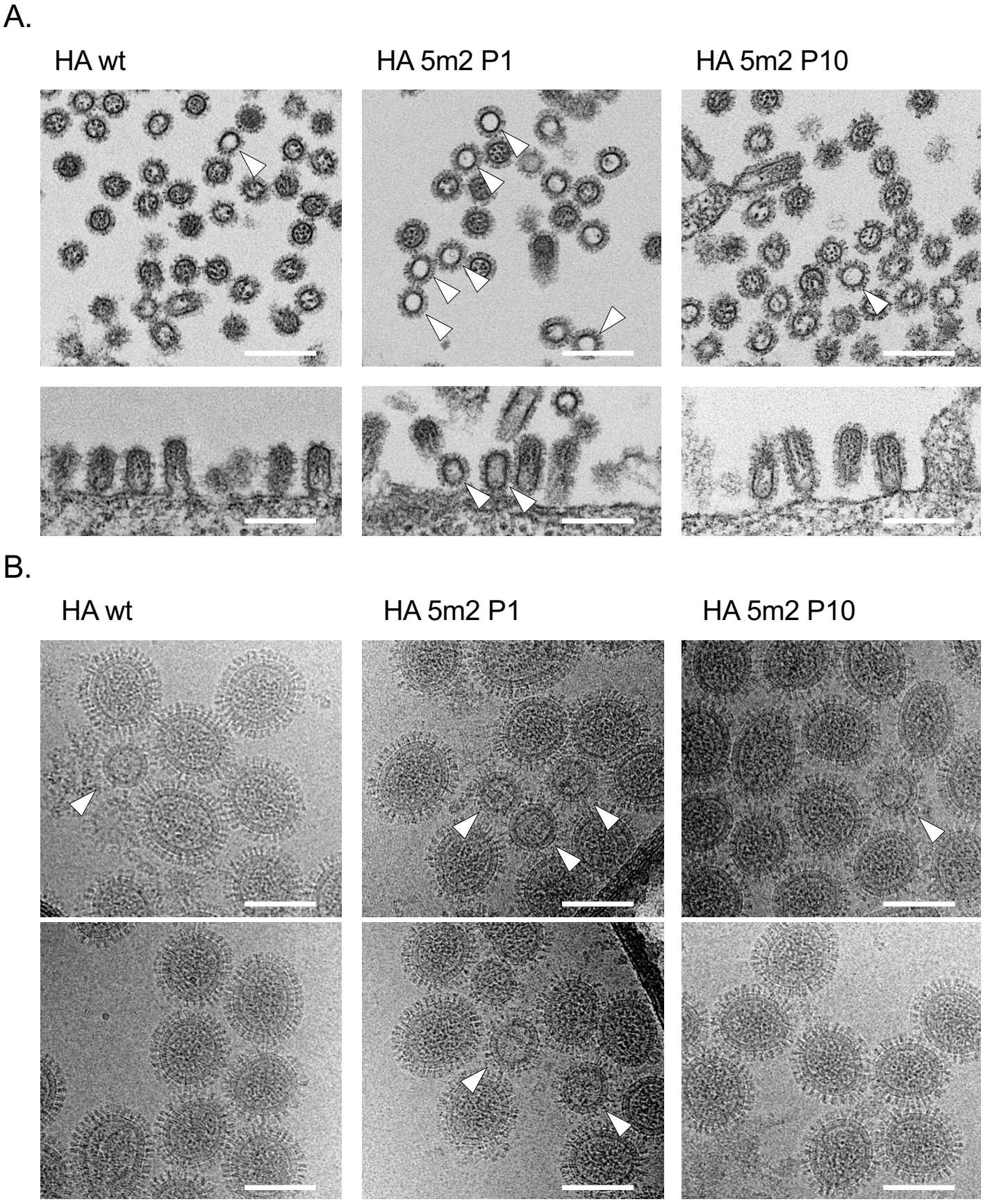

Fig 4. Morphology of HA 5m2 P1, HA5m2 P10, and wild-type viruses. (A) Ultrathin sections of viral particles budding from infected MDCK cells were observed using transverse section (upper side) and longitudinal section (lower side). Empty particles are indicated by arrowheads. Bars, 200 nm. (B) Purified virus particles were observed by cryo-TEM. Empty particles are indicated by arrowheads. Bars, 100 nm.

Figure 4

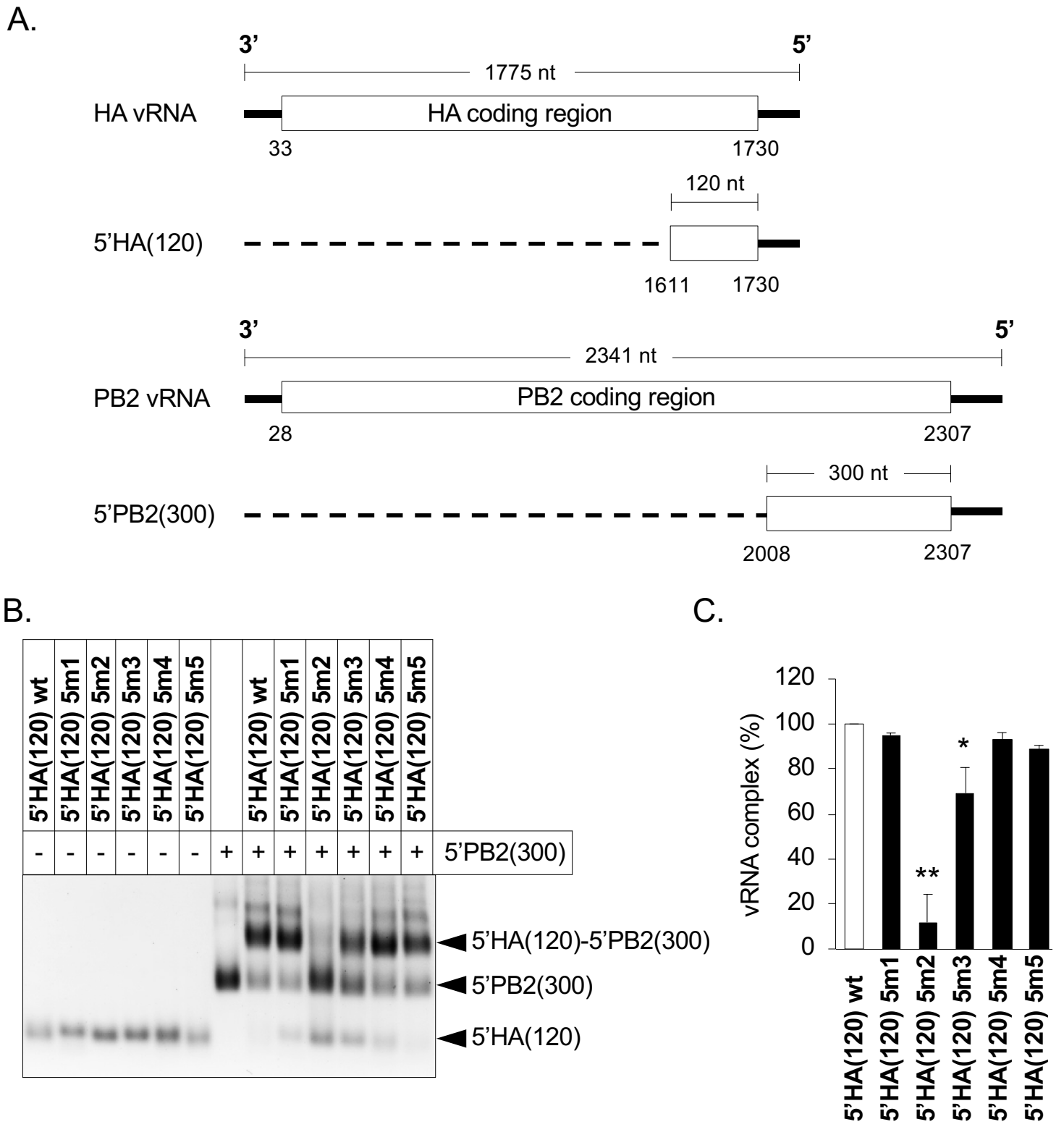

Fig 5. Gel shift assay using 5' end sequences of HA and PB2 vRNAs. (A) Schematic representation of 5'HA(120) and 5'PB2(300) vRNAs. The solid line represents the noncoding regions of vRNAs at the 3' and 5' ends. The white box represents the coding regions of the HA or PB2 proteins. The dashed line represents the deleted regions. 5'HA(120) and 5'PB2(300) contain 120 or 300 nucleotides in the coding and noncoding regions at their 5' ends, respectively. (B) The effect of silent mutations in 5'HA(120) vRNA on binding to 5'PB2(300) vRNA. 5'PB2(300) vRNA was incubated with wild-type and mutated 5'HA(120) vRNAs as indicated at the top of the gel image. Individual vRNA bands and vRNA complexes are indicated on the right. (C) Quantification of 5'HA(120)-5' PB2(300) complexes for each lane. The relative band intensity of the complex is indicated in comparison to that of the wild-type. The data represent the mean ± SD (n = 3). Dunnett's test; *P < 0.01; **P < 0.001.

Figure 5